Journal of Cluster Science (2023) 34:3047–3059
https://doi.org/10.1007/s10876-023-02446-3

ORIGINAL PAPER

A New Hybrid Organic–Inorganic Salt: *bis*(3-Aminopyridinium) Tetrachlorocobaltate(II), Application in the Synthesis of Nanostructured Co_3O_4 for Hexavalent Chromium Removal

Ichraf Chérif[1,2] · Sabri Hassen[3] · Ibtissem Jendoubi[4,5] · Fatma Mbarek[1] · Davoud Dastan[6] · Youssef Arfaoui[3] · Mounir Ferhi[7] · Mohamed Faouzi Zid[8] · Salah Ammar[1]

Received: 8 December 2022 / Accepted: 25 April 2023 / Published online: 12 May 2023

Abstract

Single crystals of *bis*(3-aminopyridinium)tetrachlorocobaltate(II) were successfully synthesized and structurally characterized using single crystal X-ray diffraction. This study shows that the structure is built on inorganic anionic and organic cationic subnetworks stabilized by Cl…Cl and antiparallel offset face to face π-π stacking interactions, respectively. The cohesion of the overall packing is ensured by N–H…Cl hydrogen bonds leading to a three dimensional network. Structural geometry optimization and gap energy determination were performed thanks to DFT calculation. Thermal decomposition of the title compound powder, at 450 °C in air atmosphere, leads to nanostructured Co_3O_4 as confirmed by X-ray powder diffraction. The obtained cobalt oxide was used as adsorbent for the removal of hexavalent chromium ions from aqueous solution. The effect of contact time was investigated and showed an unusual behavior consisting of the existence of two equilibrium plateaus at 11 $mg.g^{-1}$ and 15 $mg.g^{-1}$ which were attributed to surface heterogeneity, as elucidated by scanning electron microscopy analysis. As a consequence, the kinetic data were analyzed in steps and fitted using non linear pseudo-first order and non linear pseudo-second order models. A comparative study with other adsorbents demonstrated the potential of the synthesized Co_3O_4 via thermal decomposition of the title compound for hexavalent chromium ions removal.

Keywords Crystal structure · DFT calculation · Nanostructured cobalt oxide · Adsorption kinetic study · Removal of hexavalent chromium ions

✉ Ichraf Chérif
cherif.ichraf@yahoo.fr

✉ Davoud Dastan
d.dastan61@yahoo.com

[1] Electrochemistry, Materials and Environment Research Unit UREME (UR17ES45), Faculty of Sciences of Gabes, University of Gabes, Erriadh City, 6072 Gabes, Tunisia

[2] Higher Institute of Education and Continuous Training of Tunis, Virtual University of Tunis, Tunis, Tunisia

[3] Laboratory of Characterizations, Applications and Modeling of Materials (LR18ES08), Department of Chemistry, Faculty of Sciences of Tunis, University of Tunis El Manar, 2092 Tunis, Tunisia

[4] Faculty of Sciences of Bizerte, Carthage University, Zarzouna, 7021 Bizerte, Tunisia

[5] Faculty of Sciences of Tunis, Laboratory of Atomic Molecular Spectroscopy and Applications, 2092 Tunis, Tunisia

[6] Department of Materials Science and Engineering, Cornell University, Ithaca, NY 15850, USA

[7] Physico-Chemistry Laboratory for Mineral Materials and Their Applications, National Center for Research in Materials Sciences (CNRSM), Borj Cedria Technopole, 8027 Soliman, Tunisia

[8] University of Tunis El Manar, Faculty of Sciences of Tunis, Laboratory of Materials, Crystal Chemistry and Applied Thermodynamics, 2092 El Manar II, Tunis, Tunisia

Introduction

Weak intermolecular interactions such as hydrogen bonding, π-π stacking and Van der Waals contacts have been recognized of enormous importance in the structural arrangement and consequently in the design of hybrid organic–inorganic systems [1–4]. Furthermore, these weak interactions help to explain some physical properties like magnetism which is transmitted through intermolecular X…X contacts in $A_2[MX_4]$ compounds (A = protonated base, M = + II transition metal ion and X = Cl^- or Br^-). For example, (2-amino-3-methylpyridinium)$_2$[$CoBr_4$] (1) and (2-amino-3-methylpyridinium)$_2$[$CoCl_4$].H_2O (2) [5] compounds showed different magnetic behaviors even they crystallize in the same space group with almost similar lattice parameters. Compound (1) presents a ladder structure unlike compound (2) where the presence of a water molecule that develops O–H…Cl hydrogen bonds avoid the ladder structure formation and thus the ferromagnetic interaction observed in (1).

Among the aforementioned $A_2[MX_4]$ compounds, the family of *bis*(substituted pyridinium cations) tetrachlorocobaltate(II) formulated as (spyH)$_2$[$CoCl_4$].xH_2O presents a particular structural richness [5–13]. Review of previous published works shows that, depending on the used organic cation, different types of C/N–H…Cl interactions and π-π stacking are observed. As illustrated in Fig. 1, centrosymmetric [5–8, 10, 11] and non-centrosymmetric [9, 12] compounds were effectively synthesized. From 1997 until 2022, efforts have been made to synthesize salts of this family. The first two representative compounds were developed in 1997 and 2003 using n-dimethylaminopyridinium with n = 2 [6] and 4 [7] respectively. The n-aminopyridinium counterions were tested for n = 2 [8] and n = 4 [9]. As for n = 4, the resulting salt is non-centrosymmetric ($P2_12_12_1$ space group). In 2010, 2-amino-n-methylpyridinium cations (n = 3 and 5) [5] were investigated and showed the formation of a hydrate compound for n = 3. Several years later, a renewed interest was given to these compounds by Mghandef and co-workers [10] and Ben Moussa's research team [11] where 2-amino-5-chloropyridinium and 2,6-diaminopyridinium were exploited as organic cations, respectively. Finally, in 2022, Alotaibi et al. [12] reported the structure of a non-centrosymmetric compound with 4-tert-butylpyridinium as organic cation.

Recently, theoretical studies of hybrid organic–inorganic salts using ab initio calculation based on density functional theory (DFT) have phenomenally gained popularity. Requiring less time and leading to good agreement with experimental results, the theoretical approach proves efficient [14–16]. With regard to (spyH)$_2$[$CoCl_4$].xH_2O salts, DFT calculations were recently carried for the first time by Xu et al. (2020) on *bis*(2-aminopyridinium)tetrachlorocobaltate(II) and allowed the estimation of the first hyperpolarisability value, a key parameter for NLO application [13].

On the other hand, the conception of new coordination compounds as precursors for the synthesis of nanometric metal oxides has been recently exploited and showing promising findings. Several ligands such as Schiff base [17, 18], hydroxyterpyridine [19], bipyridine [20] as well as carboxamide [21] were successfully used in this context for the synthesis of cobalt complexes. The corresponding Co_3O_4 nanostructures afforded a wide spectrum of applications, in particular, the removal of inorganic pollutants such as Cr(VI) ions [20]. Hence, to extend the exploitation of the above mentioned synthetic approach and to better understand how n-aminopyridinium cations interact with $[CoCl_4]^{2-}$ complex, it would be interesting to test n = 3 and compare the obtained results to those that have already been published for n = 2 [8] and 4 [9]. Once crystals were collected, they may be used

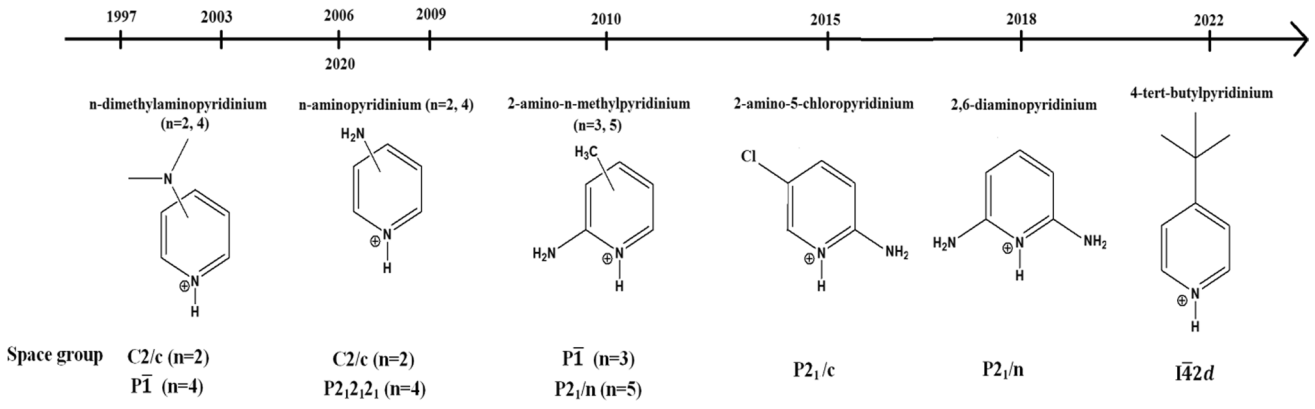

Fig. 1 Historical overview of substituted pyridinium cations used in the synthesis of (spyH)$_2$[$CoCl_4$].xH_2O compounds that crystallize in different space groups

in application as precursor for the elaboration of nanostructured cobalt oxide, efficient for the removal of Cr(VI) ions.

In the present work, an experimental and theoretical structure study of a new hybrid organic–inorganic salt: *bis*(3-aminopyridinium)tetrachlorocobaltate(II) (noted hereafter $(3\text{-}NH_2pyH)_2[CoCl_4]$) is reported. Adsorption kinetic study of Cr(VI) by the resulting cobalt oxide is also discussed on the base of non linear pseudo-first/second order models and correlated with its morphological features.

Experimental Details

Materials

All chemicals were purchased from Sigma-Aldrich and used as received: $CoCl_2.6H_2O$ (98%), 3-aminopyridine (99%), HCl (37%) and $K_2Cr_2O_7$ (99%). Distilled water was used to dilute the HCl stock solution and to prepare all the solutions for the synthesis of the title compound as well as the adsorption experiments.

Synthesis of $(3\text{-}NH_2pyH)_2[CoCl_4]$ and Co_3O_4

$CoCl_2.6H_2O$ (1 mmol) and 3-aminopyridine (2 mmol) were separately dissolved in 25 cm^3 of distilled water. The 3-aminopyridine solution was acidified with 1 cm^3 of concentrated HCl (2 M) and then mixed with Co^{2+}. The obtained solution was subjected to constant stirring at room temperature for 2 h, poured into a Petri dish and allowed to evaporate. Light blue rectangular crystals suitable for single crystal X-ray diffraction analysis were obtained after two weeks of slow evaporation. Subsequently, all crystals were collected, grinded and finally subjected to thermal treatment in a furnace at 450 °C for 4 h in air atmosphere; the cobalt oxide Co_3O_4 was identified using X-ray powder diffraction analysis as the product of this thermal decomposition.

Single Crystal X-Ray Diffraction Analysis

Good-quality single crystals of $(3\text{-}NH_2pyH)_2[CoCl_4]$ were extracted (Fig. 2) and one of them with dimensions $0.42 \times 0.36 \times 0.22$ mm was mounted at room temperature on an Enraf–Nonius CAD-4 diffractometer ($\lambda_{Mo\ K\alpha} = 0.71073$ Å).

The unit cell parameters were determined from least-squares refinement from 25 reflections in the range $10° < \theta < 15°$. Intensity data were corrected for Lorentz-polarization and absorption (ψ-scan) effects. Of the 3525 measured independent reflections in the θ range 2.46–27.16° with index ranges $-8 \le h \le 1$, $-10 \le k \le 10$ and $-17 \le 1 \le 17$, 2847 were observed with $I > 2\sigma(I)$ and used for structure refinement. The structure was solved by direct methods using the SHELXS-97 program and was refined by the full-matrix least-squares method on F^2 for 173 refined parameters using the SHELXL-97 program [22]. All non-H atoms were treated anisotropically. Carbon and nitrogen H atoms were constrained to an ideal geometry with d(C–H) = 0.93 Å, d(N–H) = 0.86 Å and $U_{iso}(H) = 1.2U_{eq}$(C or N). The residual maxima and minima in the final Fourier difference map were 1.33 and

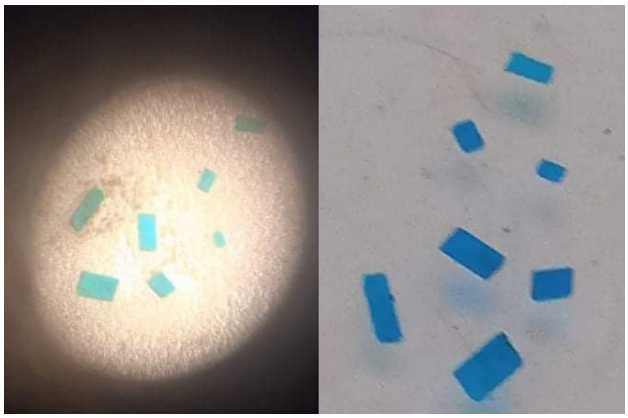

Fig. 2 Selected single crystals of $(3\text{-}NH_2pyH)_2[CoCl_4]$

Table 1 Summary of the crystal data and structure refinement for $(3\text{-}NH_2pyH)_2[CoCl_4]$

Formula	$C_{10}H_{14}Cl_4CoN_4$
M ($g.mol^{-1}$)	390.98
Crystal system	Triclinic
Space group	P-1
a (Å)	6.945(1)
b (Å)	8.503(2)
c (Å)	13.862(3)
α (°)	81.36(2)
β (°)	89.40(2)
γ (°)	80.17(2)
V ($Å^3$)	797.3(3)
Z	2
ρ_{calc} ($g.cm^{-3}$)	1.628
F(000)	394
μ (mm^{-1})	1.737
R_{int}	0.042
GOOF on F^2	1.041
R^a and ωR^b indices ($I > 2\sigma(I)$)	0.072, 0.1823
CCDC No	2175244

$^aR = (\sum||F_0|-|F_c||)/\sum|F_0|$, $^b\omega R = ((\sum[\omega(|F_0|^2-|F_c|^2)]^2)/\sum[\omega|F_0|^2]^2)^{1/2}$ *where* $\omega = 1/(\sigma^2(F_0^2)+(0.1535P)^2+0.0654P)$ *and* $P = (F_0^2+2F_c^2)/3$

– 1.76 e.Å^{-3}. A summary of the crystall ographic data and structure refinement is given in Table 1.

Computational Studies

The geometry of the title compound was optimized with the DFT method [23] using the Gaussian 09 program [24] at the B3LYP hybrid function [25, 26] with 6–311 + + G(2d,2p) basis set level [27]. Starting from the X–ray geometry as an initial guess structure, the optimization was performed with the default convergence criteria without any constraint on the geometry. Based on the optimized structure, the molecular electrostatic potential (MESP) and the frontier molecular orbital (LUMO = lowest unoccupied molecular orbital and HOMO = highest occupied molecular orbital) analyses were performed.

Characterization Techniques

The synthesis of Co_3O_4 was confirmed by X-ray powder diffraction (XRPD) using a D8 ADVANCE Bruker diffractometer with Cu Kα radiation (λ = 1.5418 Å) in the 2θ range of 10–80°. The adsorption of hexavalent chromium ions on the cobalt oxide was followed by UV-6300PC double beam spectrophotometer. The morphological characterization of the cobalt oxide was carried out with a Quanta FEG 650 model of scanning electron microscope (SEM) operating with a voltage of 20 kV.

Adsorption Experiments

Kinetic study of hexavalent chromium adsorption on the obtained Co_3O_4 was conducted at room temperature and natural pH in a time range 0–80 min. First, 100 mL of chromium aqueous solution at a concentration of 60 mg. L^{-1} was prepared using an appropriate amount of $K_2Cr_2O_7$. Then, 0.2 g of Co_3O_4 was introduced to the chromium solution under constant stirring and samples of 10 mL were taken at selected times (5, 10, 15, 20, 30, 40, 50, 60, 70 and 80 min), filtered and analyzed using UV–Vis spectrophotometer at λ_{max} = 371 nm which corresponds to the maximum absorbance of chromium solution as shown in Fig. S1. The adsorption experiments were conducted in triplicate and the adsorption capacity was calculated according to the following expression [28] where C_0, C_t, V and m are the initial concentration of Cr(VI) solution (mg.L^{-1}), the Cr(VI) concentration at time t (mg.L^{-1}), the volume of Cr(VI) solution (mL) and the Co_3O_4 mass (mg), respectively.

$$\textbf{Adsorption capacity}\ \left(\textbf{mg.g}^{-1}\right)\mathbf{q_t} = \frac{\left(\mathbf{C_0} - \mathbf{C_t}\right) * \mathbf{V}}{\mathbf{m}}$$

Results and Discussion

Single Crystal X-Ray Diffraction and DFT Calculations

The asymmetric unit of the title compound, shown in Fig. 3a, consists of two independent 3-aminopyridinium cations (noted hereafter cation 1 and cation 2 for N1 and N3 pyridinium rings, respectively) and a $[CoCl_4]^{2-}$ anion. This latter exhibits a tetrahedral geometry with Co–Cl distances ranging from 2.257(1) to 2.288(1) Å and Cl–Co–Cl angles ranging from 103.86(4) to 114.66(4) (Table 2), in agreement with similar structures previously reported for monoprotonated substituted pyridines [5–13]. The

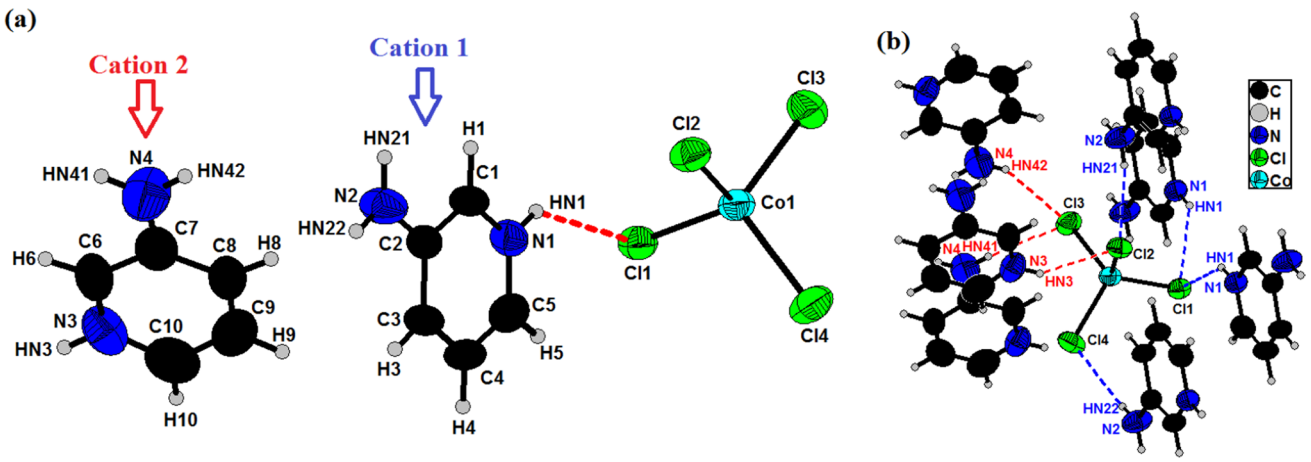

Fig. 3 **a** Asymmetric units of the title compound with the atomic numbering scheme. The thermal ellipsoids are drawn at the 50% probability level at 298 K for non-H atoms **b** Anionic unit environment ensured by H-bonds developed by cation 1 (blue dashed bonds) and cation 2 (red dashed bonds)

Table 2 Selected experimental and theoretical bond lengths and angles for $(3\text{-}NH_2pyH)_2[CoCl_4]$

$[CoCl_4]^{2-}$ unit					
Bond lengths (Å)			Bond angles (°)		
	Exp	Cal		Exp	Cal
			Cl(1)-Co(1)-Cl(2)	108.83(4)	110.16
Co(1)-Cl(1)	2.2570(11)	2.328	Cl(3)-Co(1)-Cl(2)	103.86(4)	110.53
Co(1)-Cl(2)	2.2880(10)	2.441	Cl(3)-Co(1)-Cl(4)	111.08(5)	115.21
Co(1)-Cl(3)	2.2801(11)	2.297	Cl(1)-Co(1)-Cl(4)	114.66(4)	110.27
Co(1)-Cl(4)	2.2570(11)	2.288	Cl(1)-Co(1)-Cl(3)	106.76(4)	110.27
			Cl(4)-Co(1)-Cl(2)	108.83(4)	99.95
3-aminopyridinium cations					
Bond lengths (Å)			Bond angles (°)		
Cation 1					
	Exp	Cal		Exp	Cal
N(1)-C(1)	1.338(5)	1.329	C(1)-N(1)-C(5)	124.0(4)	123.8
N(1)-C(5)	1.343(6)	1.339	N(1)-C(1)-C(2)	119.4(3)	120.6
N(2)-C(2)	1.352(5)	1.373	N(2)-C(2)-C(1)	120.7(4)	119.1
C(1)-C(2)	1.390(5)	1.396	N(2)-C(2)-C(3)	122.1(4)	124.0
C(2)-C(3)	1.397(5)	1.401	C(1)-C(2)-C(3)	117.2(4)	116.9
C(3)-C(4)	1.361(6)	1.388	C(4)-C(3)-C(2)	121.0(4)	120.4
C(4)-C(5)	1.365(6)	1.381	C(3)-C(4)-C(5)	120.4(4)	120.0
			N(1)-C(5)-C(4)	118.0(4)	118.3
Cation 2					
	Exp	Cal		Exp	Cal
N(3)-C(6)	1.327(7)	1.330	C(6)-N(3)-C(10)	125.5(4)	123.8
N(3)-C(10)	1.346(8)	1.342	N(3)-C(6)-C(7)	119.0(5)	120.6
N(4)-C(7)	1.348(7)	1.368	N(4)-C(7)-C(6)	119.6(5)	128.8
C(6)-C(7)	1.382(7)	1.405	N(4)-C(7)-C(8)	123.6(5)	124.4
C(7)-C(8)	1.398(7)	1.402	C(6)-C(7)-C(8)	116.7(5)	116.7
C(8)-C(9)	1.356(7)	1.385	C(9)-C(8)-C(7)	121.4(5)	120.4
C(9)-C(10)	1.359(8)	1.380	C(8)-C(9)-C(10)	120.7(5)	120.1
			N(3)-C(10)-C(9)	116.6(5)	118.2

$[CoCl_4]^{2-}$ tetrahedron is almost perfect with a τ_4 geometric parameter for four-coordinate compounds of 0.95 as proposed by Yang et al. [29]. This parameter was calculated for *bis*(2-aminopyridinium)tetrachlorocobaltate(II) and *bis*(4-aminopyridinium)tetrachlorocobaltate(II) and shows relatively more distorted anionic units with τ_4 values of 0.91 and 0.94, respectively. It is worth noting that the slight deviation from ideal tetrahedral geometry is attributed to N–H…Cl interactions between the tetrachlorocobaltate(II) complex and $(3\text{-}NH_2pyH)^+$ (Table 3) where chloride ions Cl1, Cl2 and Cl3 act as doubly H-bond acceptors unlike Cl4 which is simply acceptor. A $[CoCl_4]^{2-}$ unit is thus surrounded by seven 3-aminopyridinium cations, as shown in Fig. 3b.

The optimization of bonding parameters, namely bond lengths and angles, for the title compound (Table 2) leads

Table 3 Hydrogen bond geometry (Å, °) for $(3\text{-}NH_2pyH)_2[CoCl_4]$

D-H…A	D-H	H…A	D…A	D-H…A
N1-HN1…Cl1^{i}	0.86	2.667	3.306(4)	132
N1-HN1…Cl1	0.86	2.706	3.374(4)	136
N2-HN21…Cl2^{ii}	0.86	2.759	3.488(4)	144
N2-HN22…Cl4^{iii}	0.86	2.788	3.619(4)	163
N3-HN3…Cl2^{iv}	0.86	2.481	3.232(4)	146
N4-HN41…Cl3^{v}	0.86	2.570	3.399(6)	162
N4-HN42…Cl3^{ii}	0.86	2.842	3.633(5)	154

Symmetry codes: (i) −x + 2, −y, −z + 1; (ii) −x + 1, −y, −z + 1; (iii) −x + 1, −y + 1, −z + 1; (iv) x,y,z + 1; (v) x−1,y,z + 1

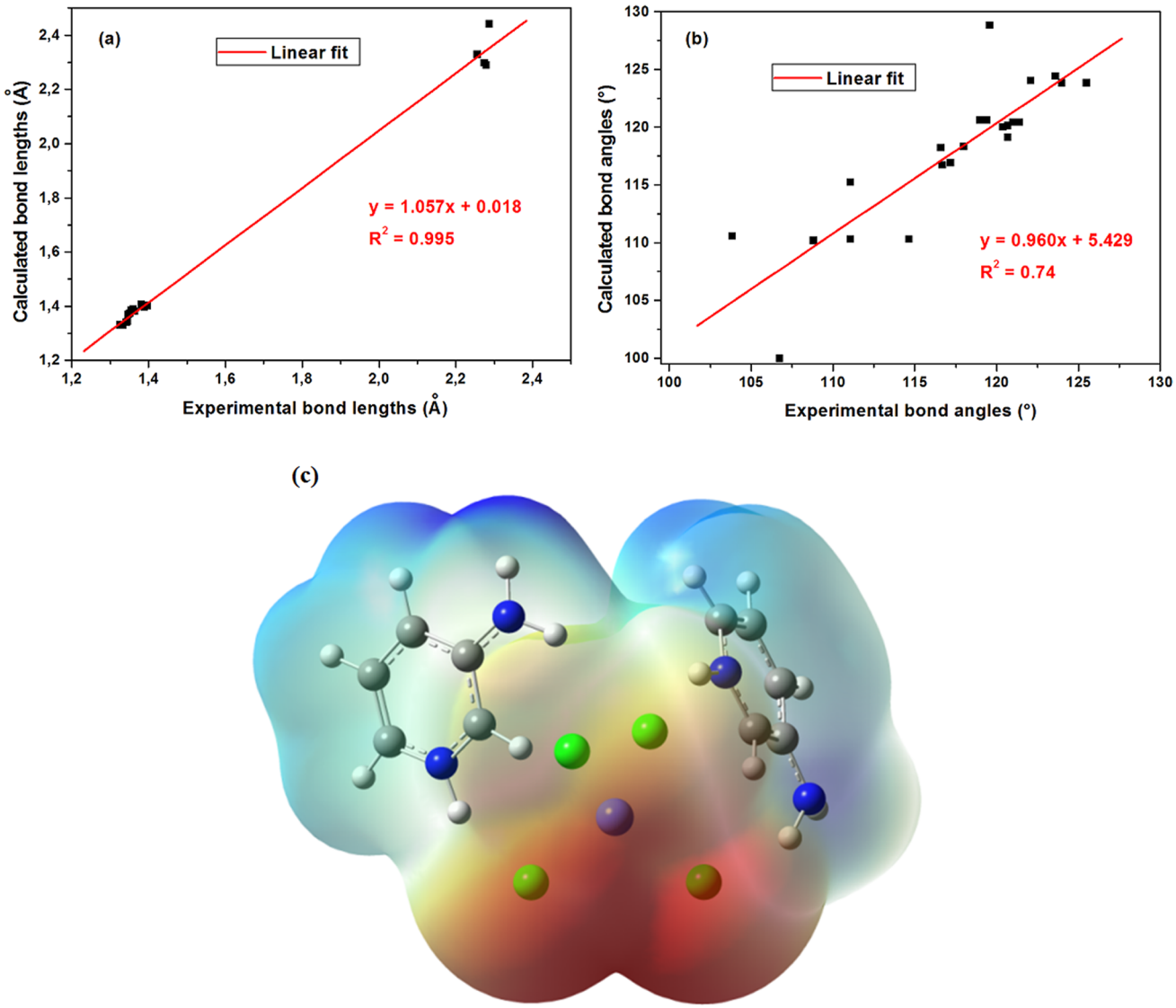

Fig. 4 **a, b** Graphical correlation between experimental and calculated bond lengths and angles, respectively **c** The molecular electrostatic potentials (MEPs) map of the title compound

to consistent values with data deduced from X-ray diffraction analysis. The graphical correlation between experimental and theoretical values is shown in Fig. 4a, b with an R^2 coefficient of 0.995 and 0.74 for bond lengths and angles, respectively. The slight differences observed for both values are attributed to the fact that theoretical calculations were performed in the gas phase. However, to predict possible inter/intra-molecular interactions via H-bonds, the positive and negative sites were identified through the molecular electrostatic potential (MESP) analysis. The red and blue regions correspond to the most nucleophilic (electron-rich region) and electrophilic (electron-deficient region) sites, respectively. The analysis of the MESP map (Fig. 4c) shows that the chlorides are the negative sites since they possess higher maximum potential values which is in accordance with the experimental results recorded in Table 3, where Cl^- anions act as acceptors of H-bonds.

The anionic framework of the title compound can be described as layers parallel to (010) by considering the shortest Cl…Cl contacts (3.723(2) and 4.044(2) Å) (Fig. 5a). These separation values, taken into account when magnetic properties are explored, are in the same range as those found by Ben Moussa et al. (3.889(2) and 3.986(2) Å) [11] but significantly less than 4.119(2) and [4.205(2) and 4.349(2)] for compounds involving 2-amino-n-methylpyridinium cations (n = 3 and 5, respectively) [5]. The shortest Co… Co distances are 6.945(1) and 6.123(3) Å along a and c axes, respectively (Fig. 5a). For *bis*(n-aminopyridinium) tetrachlorocobaltate(II) salts (n = 2 and 4), isomers of

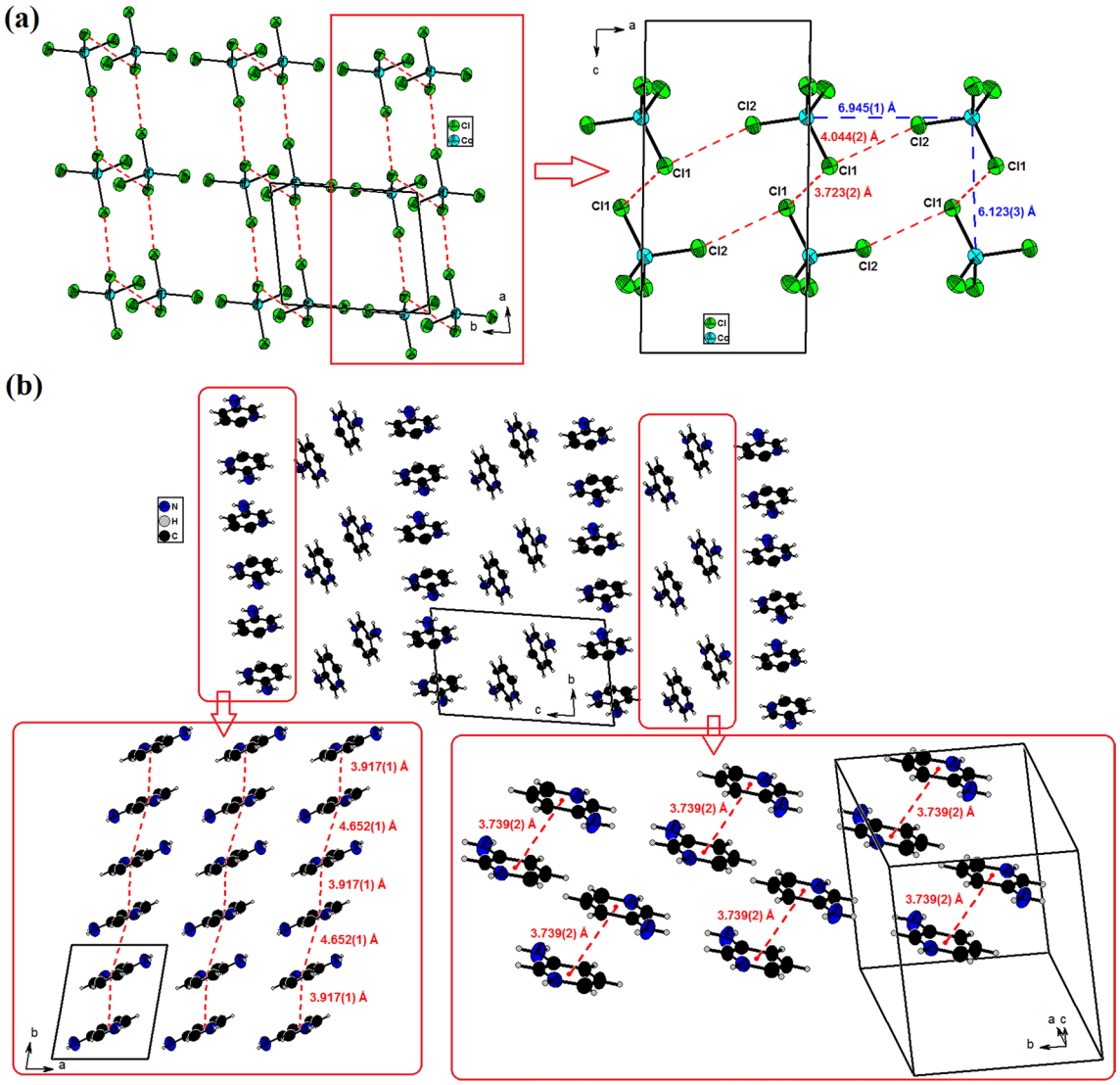

Fig. 5 The title compound **(a)** anionic framework defined based on the shortest Cl…Cl contacts **(b)** illustration of π-π stacking interactions with centroid to centroid distances

the title compound for which n = 3, $[CoCl_4]^{2-}$ layers parallel to (110) for n = 2 and (001) for n = 4 are observed with Cl…Cl separations of [4.113(3)– 4.713(1) Å] and [4.391(1)– 4.452(1) Å] and shortest Co…Co distances of [6.890(1)– 8.147(1) Å] and [7.701(1)–7.172(1) Å] respectively as shown in Fig. S2(a, b).

As far as organic cations are concerned, their geometric parameters (Table 2) are very close and comparable to previously reported works including non-coordinating $(3\text{-}NH_2pyH)^+$ [30]. Protonation of the heterocycle nitrogen (N1 and N3) occurred as expected and is confirmed by the opening of the C1-N1-C5 (124.0(5)°) and C6-N3-C10 (125.5(4)°) angles compared to the neutral 3-aminopyridine (117.7(1)°) [31]. The angle between the rings mean planes of cations 1 and 2 is 65.59° as shown in Fig. S3. Two sets of offset face to face and antiparallel π-π stacking interactions were observed: parallel mean planes of cation's 1 pairs are spaced by 3.453 Å with a centroid to centroid distance of 3.739(2) Å. Cations 2, on the other hand, define chains developed along *b* axis with centroid to centroid distances of 3.917(1) Å and 4.652(1) Å and interplanar separations of 3.538 Å and 3.493 Å, respectively (Fig. 5b). These two types of cationic stacks are further hydrogen bonded to $[CoCl_4]^{2-}$ units.

For the overall hybrid structure, organic and inorganic components are held together through N–H… Cl hydrogen bonds where cations 1 and 2 interact with three and two $[CoCl_4]^{2-}$ units, respectively, as shown in Fig. 6. A careful examination of the *bis*(n-aminopyridinium)tetrachlorocobaltate(II) (n = 2, 3 and 4) structures

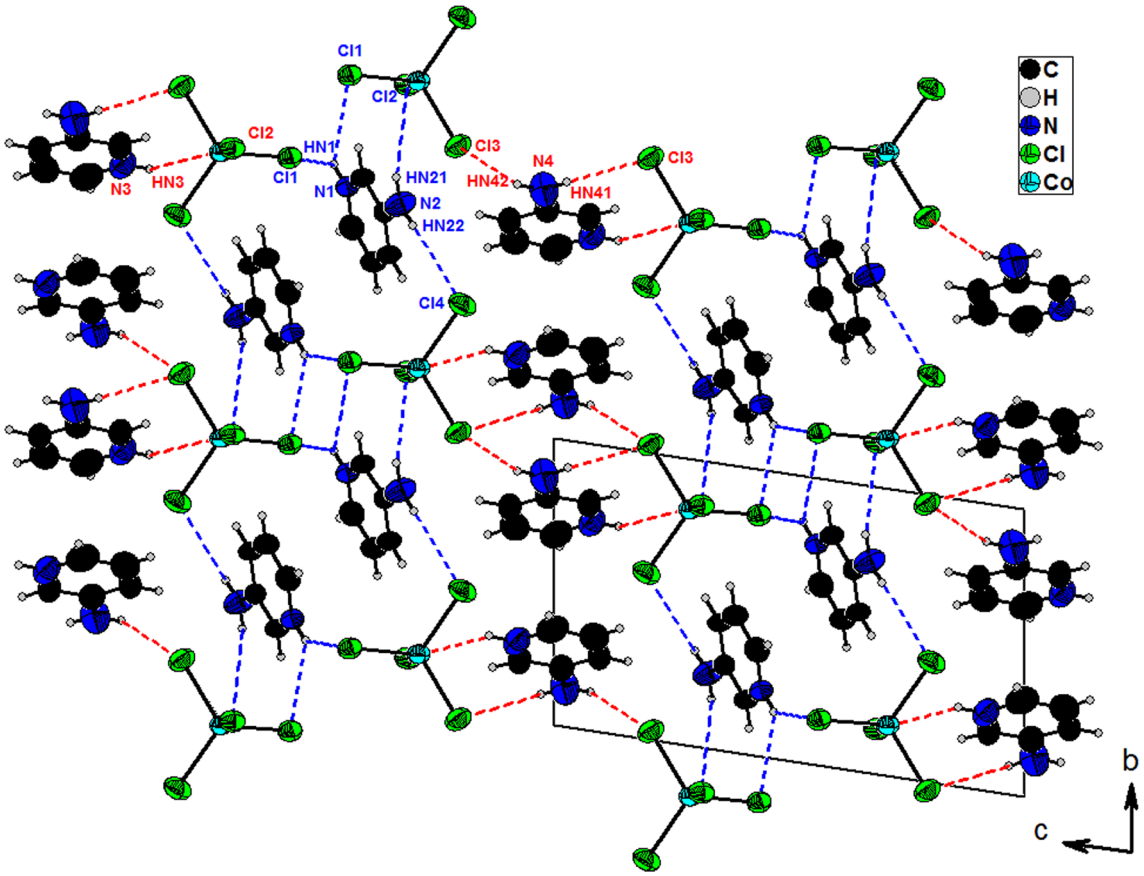

Fig. 6 Illustration of the crystal packing of the title compound viewed along the a axis. Dashed lines correspond to the hydrogen bonds developed between cations 1 (blue) and cations 2 (red) with $[CoCl_4]^{2-}$ units

crystallizing in different systems (monoclinic, orthorhombic and triclinic, respectively) reveals that they exhibit different supramolecular features. Unlike the title compound, neither the 2-aminopyridinium nor the 4-aminopyridinium corresponding compounds have π-π interactions. As far as N–H…Cl H-bonds are concerned, several arrangements were observed. For the three compounds, each hydrogen of the exocyclic amino group develops a single interaction with chloride ions connecting thus three $[CoCl_4]^{2-}$ units for n = 3 and two units for both n = 2 and 4 (Fig. S4). In contrast, the hydrogen bound to the ring nitrogen leads to single and bifurcated interactions. For the title compound (n = 3) and n = 4, which are constructed by two crystallographically independent organic cations, both interaction types exist; the bifurcated ones link two anionic units for n = 3 and interact with two chloride from the same unit for n = 4. For n = 2, however, the Co atom lies on a crystallographic twofold rotation axis and the asymmetric unit contains thus a 2-aminopyridinium cation where the nitrogen of the pyridine ring is singly H-bounded to Cl atom. Therefore, it is quite clear that the interaction between anionic-cationic networks differs from one compound to another depending on the organic base used *i.e.* the three possible positions of the $–NH_2$ group.

To estimate the energy gap value of the title compound, frontier molecular orbital analysis was performed as shown in Fig. 7. The HOMO orbital is localized in the $[CoCl_4]^{2-}$ anion which may thus act as an electron donor, whereas the LUMO orbital is localized in the 3-aminopyridinium cation that can perform as an electron acceptor. The energy gap values, deduced from the expressions: $E_{LUMO}(\alpha) - E_{HOMO}(\alpha)$ and $E_{LUMO}(\beta) - E_{HOMO}(\beta)$, are found as 3.74 and 3.41 eV, respectively. These values are comparable to those found in similar compounds: $(C_{13}H_{22}N)_2[CoBr_4]$ [32] and $(C_6H_9N_2)_2[CoCl_4]$ [33] synthesized by Dgachi et al. and indicate that the title compound exhibits a semiconductor behavior [32–36].

X-Ray Powder Diffraction Analysis

The thermogravimetric analysis was not performed to determine the appropriate calcination temperature of the title compound leading to pure Co_3O_4 phase. Instead, the authors relied on the literature that dealt with the synthesis

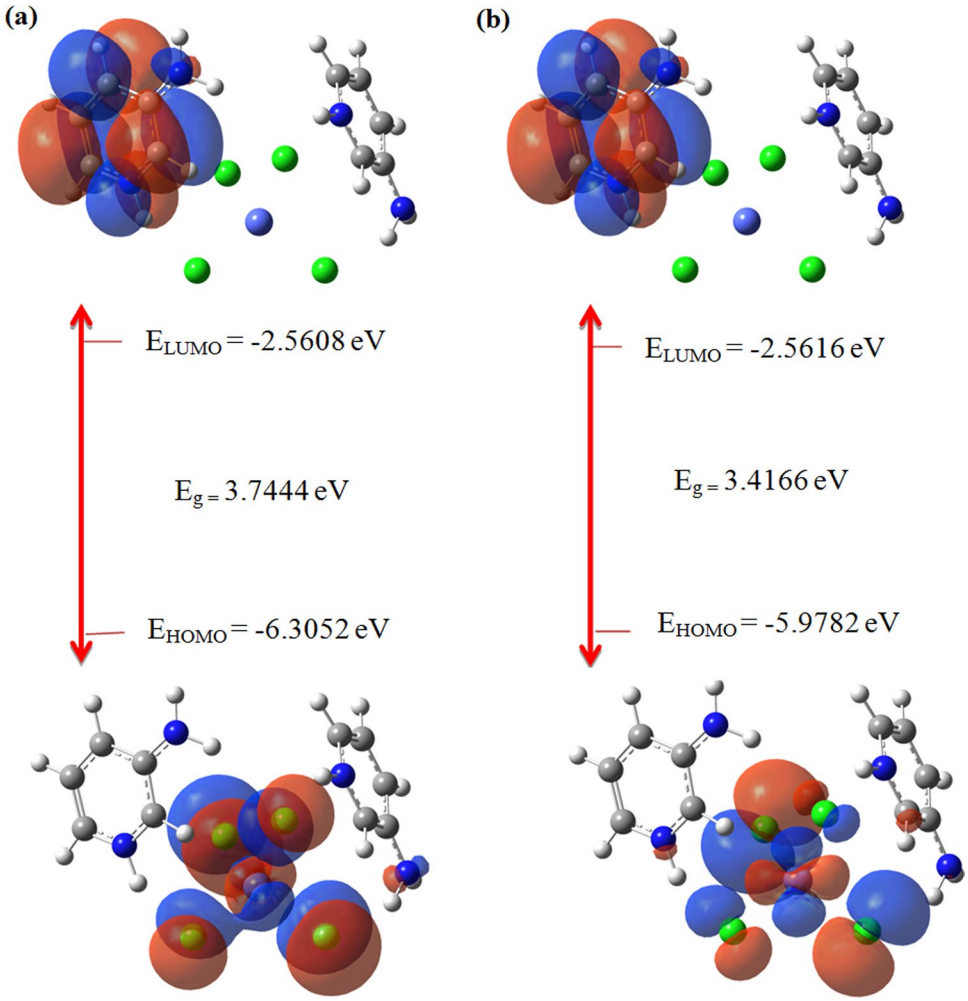

Fig. 7 Calculated HOMO–LUMO energies and energy gap values of the title compound (**a**) alpha α (**b**) beta β

of Co_3O_4 by thermal decomposition of organic-based cobalt complexes. Specifically, Ben Salah et al. [37] conducted a detailed study of the thermal behavior of the chiral $[R\text{-}(C_8H_{12}N)_3][CoCl_4]Cl$ using TGA-DTA and temperature-dependent X-ray powder diffraction and found that Co_3O_4 was formed during the last step of thermal decomposition between 350 and 550 °C. Thus, as a first attempt, the title compound was treated at a temperature of 450 °C for 4 h and the resulting product was systematically subjected to X-ray powder diffraction analysis to identify it. With regard to $(spyH)_2[CoCl_4].xH_2O$ compounds, it has to be noted that a deeper study of their thermal behavior has never been done.

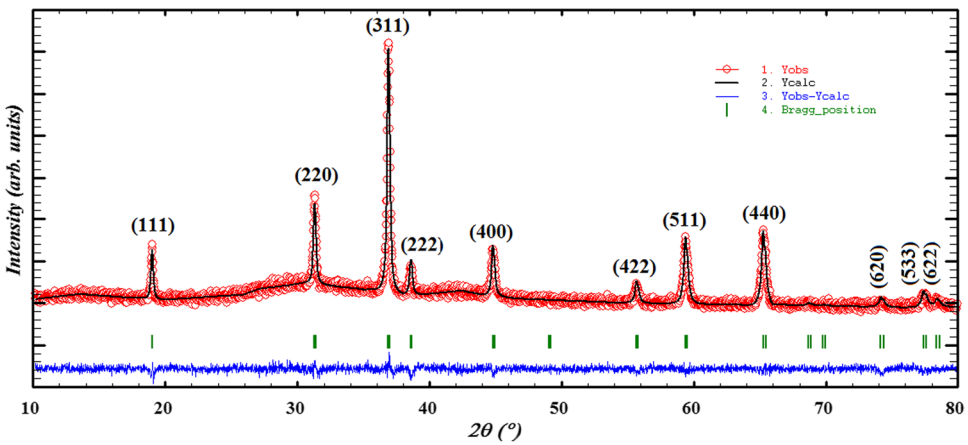

Fig. 8 "Profile Matching" result for Co_3O_4 powder pattern

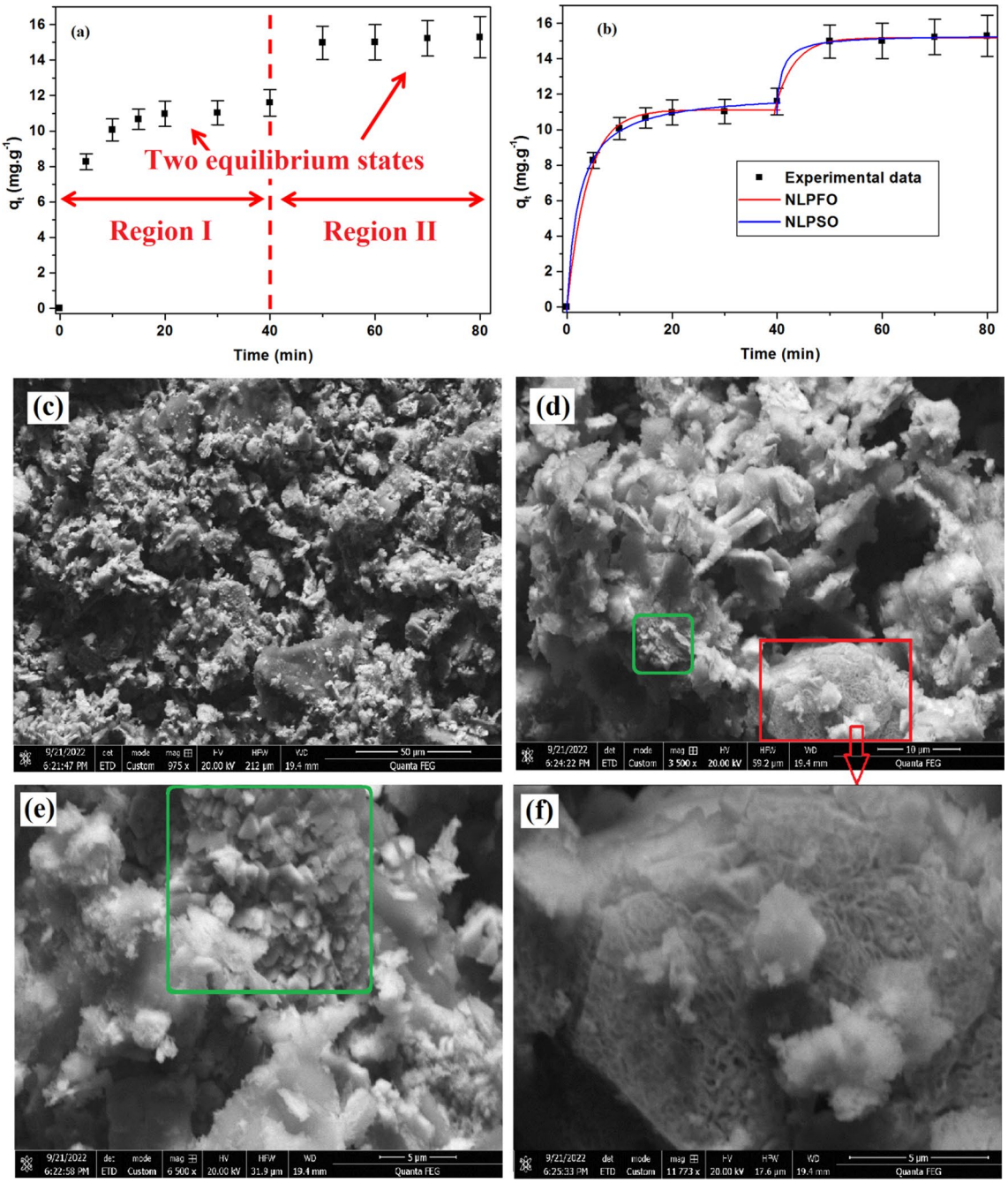

Fig. 9 **a** Kinetic study of the adsorption capacity of Cr(VI) by Co_3O_4 (error bars represent the standard deviation of triplicate measurements) **b** NLPFO and NLPSO kinetic models applied for the adsorption modeling of Cr(VI) by Co_3O_4 **c–f** SEM images of Co_3O_4 with different magnifications

Xu et al. (2020) [13] and Alotaibi et al. (2022) [12] have recently reported the thermal stability of $(C_5H_7N_2)_2[CoCl_4]$ (I) and $(C_9H_{14}N)_2[CoCl_4]$ (II) respectively under N_2 atmosphere. TGA curves revealed a final constant weight plateau after 725 °C for (I) and 625 K for (II), however, no further characterizations were done to identify the obtained products at these temperatures.

Figure 8 depicts the X-ray powder diffraction pattern of the obtained black powder after calcination of the title compound at 450 °C for 4 h. Diffraction peaks identified at $2\theta = 19.1$, 31.2, 36.8, 38.5, 44.8, 55.6, 59.3, 65.2 and 77.3° are attributed to the spinel Co_3O_4 phase according to the JCPDS card No. 42–1467. Besides, a "Profile Matching" refinement carried out in this direction leads to a

Table 4 Kinetic parameters deduced from NLPFO and NLPSO models

	Parameters	0–40 min	40–80 min
NLPFO $q_t = q_e(1\text{-}e^{-k_1 t})$ [40]	q_e ($mg.g^{-1}$)	11.12 ± 0.14	15.18 ± 0.08
	k_1(min^{-1})	0.26 ± 0.02	0.28 ± 0.07
	χ^2	0.07	0.02
	Δq(%)	2.56	0.68
NLPSO $q_t = \frac{k_2 q_e^2 t}{1+k_2 q_e t}$ [40]	q_e ($mg.g^{-1}$)	12.15 ± 0.14	15.34 ± 0.11
	k_2 ($g.mg^{-1}.min^{-1}$)	0.036 ± 0.003	0.22 ± 0.05
	χ^2	0.02	0.01
	Δq(%)	1.53	0.47

q_e, k_1 and k_2 are the adsorption capacity at equilibrium ($mg.g^{-1}$), the kinetic rate constants for NLPFO (min^{-1}) and NLPSO ($g.mg^{-1}.min^{-1}$) models respectively

$\chi^2 = \sum \frac{(q_{t,exp}-q_{t,cal})^2}{q_{t,cal}}$; $SD = \Delta q(\%) = \sqrt{\frac{1}{n-1}\sum\left[\frac{q_{t,exp}-q_{t,cal}}{q_{t,exp}}\right]^2} \times 100$

good agreement between theoretical and experimental data ($R_p = 5.43$, $R_{wp} = 6.94$ and $\chi^2 = 1.24$) without additional peaks as shown in Fig. 8. Scherrer equation, $D = (k\lambda)/(\beta\cos\theta)$ (k, λ, β and θ are the shape factor (taken as 0.9), the X-ray wavelength (λ = 1.5418 Å), the full width at half maximum (FWHM) and the Bragg angle of the diffraction peak, respectively) [38], was applied for the most intense diffraction peak to estimate the crystallite's size; a value of $D \approx 40$ nm was found.

Adsorption Experiments of Cr(VI) by Nanostructured Co_3O_4

Figure 9a shows the adsorption capacity kinetic study results (q_t *vs* t). Two equilibrium plateaus at $q_t = 11$ mg. g^{-1} and 15 $mg.g^{-1}$ were reached after 20 min and 50 min as contact time, respectively. In the first five minutes, the adsorption is rapid ($q_t = 8.23$ $mg.g^{-1}$) and then gradually increases between 5 and 20 min to reach the first equilibrium state over ≈ 20 min. After 40 min, the adsorption increases again from 40 to 50 min to achieve the final equilibrium state ($q_t = 15$ $mg.g^{-1}$). This unusual behavior was also observed by Bizi (2020) [39] for the sulfamethoxazole adsorption on activated carbon (AC) and was attributed to texture heterogeneity of AC in terms of pore's size (intraparticle diffusion in micropores followed by diffusion in mesopores). In order to check if this is also our case, SEM images of Co_3O_4 powder with different magnifications were recorded as shown in Figs. 9c–f. These latter revealed two types of clusters as pointed in Fig. 9d using green and red rectangles (Fig. 9e–f). This heterogeneity leads thus to a two-step adsorption process. To accurately model the experimental data from 0 to 40 min (Region I) and 40 to 80 min (Region II), two-step fitting using non linear pseudo-first order (NLPFO) and non linear pseudo-second order (NLPSO) kinetic models was applied. The obtained results, illustrated in Fig. 9b and gathered in Table 4, showed that the NLPSO model provided a better fit for both regions based on χ^2 [40] and standard deviation Δq [40] values.

A comparative study of our findings with those reported in the literature for different nanometric metal oxides including iron, copper and nickel oxides [41–43] shows promising adsorptive properties for hexavalent chromium ions in terms of equilibrium time and adsorption capacity (Table 5). Indeed, for Cr^{6+} and adsorbent concentrations of 60 $mg.L^{-1}$ and 2 $g.L^{-1}$ respectively, the synthesized Co_3O_4 by thermal decomposition of the title compound exhibits the highest adsorption capacity of 15 $mg.g^{-1}$ compared to 10 $mg.g^{-1}$ for Fe_3O_4-NPs [41] and 7.8 $mg.g^{-1}$ for NiO-NPs [43]. Besides, for NiO-NPs, the obtained value of 7.8 $mg.g^{-1}$ was reached after 30 min. After the same contact time, our compound presents a q_e value of 11 mg. g^{-1} which is always greater than 7.8 $mg.g^{-1}$. For CuO–NPs [42], a lower amount of adsorbent (1.6 $g.L^{-1}$) was sufficient to achieve nearly the same q_e, however, it required a contact time of 180 min which is more than three times the obtained value for Co_3O_4 (50 min).

Conclusion

The reaction of cobalt(II) salt with 3-aminopyridine in acidic medium resulted in the synthesis of $(3\text{-}NH_2pyH)_2[CoCl_4]$. On the light of the structural study, the crystal packing was found to be governed by weak intermolecular interactions involving H-bonds, π-π stacking and Van der Waals forces. These interactions were of great interest in

Table 5 Comparative study with different adsorbent used for hexavalent chromium removal

Adsorbent	Adsorption experiment conditions				q_e ($mg.g^{-1}$)	Reference
	pH	[adsorbent] ($g.L^{-1}$)	[Cr^{6+}] (mg. L^{-1})	Contact time (min)		
Fe_3O_4	3.5	2	60	---	10	[41]
CuO	3	1.6	60	180	≈ 14.8	[42]
NiO	4.7	2	60	30	7.8	[43]
Co_3O_4	Natural pH	2	60	50	15	This study

controlling the final arrangement and explained the structural variety observed with n = 2 and 4. Structural optimization using DFT calculations showed good agreement with experimental data. The energy gap of the title compound was calculated, suggesting a semiconductor behavior. The tetrachlorocobaltate(II) salt was then treated at 450 °C leading to Co_3O_4 powder which was tested for the removal of hexavalent chromium ions by adsorption. The kinetic study of the adsorption process, described by the pseudo-second-order model, showed that the adsorption capacity reached 15 $mg.g^{-1}$ after an equilibrium time of 50 min. These results show that the synthesized tetrachlorocobaltate(II) salt involving 3-aminopyridinium cations has promising potential as precursor for the elaboration of nanostructured Co_3O_4 to treat contaminated solutions with hexavalent chromium ions.

Supplementary Data

CCDC No. 2175244 contain the supplementary X-ray crystallographic data for the structure of (C5H7N2)2[CoCl4] in CIF format. Copies of this information may be obtained free of charge from The Director, CCDC, 12 Union Road, CAMBRIDGE CB2 1EZ, UK (fax: +44-1223-336-033; e-mail: deposit@ccdc.cam.ac.uk or http://www.ccdc.cam.ac.uk).

Supplementary Information The online version contains supplementary material available at https://doi.org/10.1007/s10876-023-02446-3.

Acknowledgements This work was supported by the Ministry of Higher Education and Scientific Research of Tunisia.

Author contribution IC: Conceptualization – single crystal structure determination – formal analysis—writing original draft—editing. SH, IJ and YA: Theoretical calculation – writing review. FM: Adsorption experiments—formal analysis. DD: Writing review—editing. MF: Morphological investigation – writing review—editing. MFZ: Single crystal X-ray diffraction data collection – discussion. SA: Discussion – writing review.

Declarations

Conflict of interest There is no conflict of interest related to this study.

References

1. S. Upreti and A. Ramanan (2006). *Cryst. Growth Des.* **6** (9), 2066–2071. https://doi.org/10.1021/cg0601610.
2. C. B. Aakeröy and D. S. Leinen, Hydrogen-bond assisted assembly of organic and organic-inorganic solids,. Crystal Engineering: From Molecules and Crystals to Materials. Springer, Dordrecht, pp 89–106.
3. J. Zhao, F. Chen, Y. Han, H. Chen, Z. Luo, H. Tian, Y. Zhao, A. Ma, and L. Zhu (2018). *Molecules* **23** (6), 1397–1410. https://doi.org/10.3390/molecules23061397.
4. M. L. Nisbet, Y. Wang, and K. R. Poeppelmeier (2020). *Cryst. Growth Des.* **21** (1), 552–562. https://doi.org/10.1021/acs.cgd.0c01355.
5. D. J. Carnevale, C. P. Landee, M. M. Turnbull, M. Winn, and F. Xiao (2010). *J. Coord. Chem.* **63** (13), 2223–2238. https://doi.org/10.1080/00958972.2010.502230.
6. J. M. Land, R. G. Baughman, and C. A. Hester (1997). *Acta Cryst.* https://doi.org/10.1107/S0108270197099435.
7. S. Haddad, A. Vij, and R. D. Willett (2003). *J. Chem. Crystallogr.* **33** (4), 245–251. https://doi.org/10.1023/A:1023872925437.
8. S. R. Jebas, T. Balasubramanian, and M. E. Light (2006). *Acta Cryst.* **E62** (8), m1818–m1819. https://doi.org/10.1107/S1600536806026213.
9. S. R. Jebas, A. Sinthiya, B. Ravindran Durai Nayagam, D. Schollmeyer, and S. A. C. Raj (2009). *Acta Cryst.* https://doi.org/10.1107/S1600536809013270.
10. M. Mghandef and H. Boughzala (2015). *Acta Cryst.* **E71** (5), 555–557. https://doi.org/10.1107/S2056989015007707.
11. O. Ben Moussa, H. Chebbi, and M. F. Zid (2018). *Acta Cryst.* https://doi.org/10.1107/S2056989018003171.
12. A. A. Alotaibi, C. Ayari, E. Bajuavfir, A. Ahmad, F. Al-Nahdi, A. M. Alswieleh, K. L. Alotaibi, J. Mi, C. Ben Nasr, and M. H. Mrad (2022). *Opt. Spectrosc. Thermal Anal. Cryst.* **12** (2), 140–157. https://doi.org/10.3390/cryst12020140.
13. Y. L. Xu, J. Zhang, L. S. Chen, Y. Y. Zeng, J. R. Zhou, C. L. Ni, and W. X. Zheng (2020). *J. Mol. Struct.* **1222**, 128902–128907. https://doi.org/10.1016/j.molstruc.2020.128902.
14. A. Kaiba, M. H. Geesi, Y. Riadi, E. O. Ibnouf, T. A. Aljohani, and P. Guionneau (2021). *J Solid State Chem*. https://doi.org/10.1016/j.jssc.2021.122587.
15. A. Timoumi, D. Dastan, B. Jamoussi, K. Essalah, O. Alsalmi, N. Bouguila, H. Abassi, R. Chakroun, Z. Shi, and Ş Ţălu (2022). *Mol.* **27** (19), 6151. https://doi.org/10.3390/molecules27196151.
16. S. Hadaoui, Z. Ouerghi, S. Elleuch, and R. Kefi (2022). *J Struct Mol*. https://doi.org/10.1016/j.molstruc.2021.131441.
17. Z. Abbasi, M. Salehi, A. Khaleghian, and M. Kubicki (2018). *Appl. Organomet. Chem.* **32** (11), e4542. https://doi.org/10.1002/aoc.4542.
18. E. M. M. Ibrahim, L. H. Abdel-Rahman, A. M. Abu-Dief, A. Elshafaie, S. K. Hamdan, and A. M. Ahmed (2018). *Mater. Res. Bull.* **99**, 103–108. https://doi.org/10.1016/j.materresbull.2017.11.002.
19. B. Z. Momeni, F. Rahimi, and F. Rominger (2018). *J. Inorg. Organomet. Polym. Mater.* **28** (1), 235–250. https://doi.org/10.1007/s10904-017-0706-6.
20. Z. Razmara and E. Sanchooli (2019). *J. Inorg. Organomet. Polym. Mater.* **29** (6), 2090–2102. https://doi.org/10.1007/s10904-019-01168-2.
21. S. Meghdadi, M. Amirnasr, M. Zhiani, F. Jallili, M. Jari, and M. Kiani (2017). *Electrocatalysis* **8** (2), 122–131. https://doi.org/10.1007/s12678-016-0345-7.
22. G. M. Sheldrick (2008). *Acta Cryst. A* **64**, 112–122.
23. R. Gara, M. O. Zouaghi, L. M. H. Alshandoudi, and Y. Arfaoui (2021). *J. Mol. Model.* **27** (5), 1–12. https://doi.org/10.1007/s00894-021-04729-w.
24. Gaussian 09, Revision A.1, M. J. Frisch, G. W. Trucks, H. B. Schlegel, G. E. Scuseria, M. A. Robb, J. R. Cheeseman, G. Scalmani, V. Barone, B. Mennucci, G. A. Petersson, H. Nakatsuji, M. Caricato, X. Li, H. P. Hratchian, A. F. Izmaylov, J. Bloino, G. Zheng, J. L. Sonnenberg, M. Hada, M. Ehara, K. Toyota, R. Fukuda, J. Hasegawa, M. Ishida, T. Nakajima, Y. Honda, O. Kitao, H. Nakai, T. Vreven, J. A. Montgomery, Jr., J. E. Peralta, F. Ogliaro, M. Bearpark, J. J. Heyd, E. Brothers, K. N. Kudin, V. N. Staroverov, R. Kobayashi, J. Normand, K. Raghavachari, A. Rendell, J. C. Burant, S. S. Iyengar, J. Tomasi, M. Cossi, N. Rega, J. M. Millam, M. Klene, J. E. Knox, J. B.

Cross, V. Bakken, C. Adamo, J. Jaramillo, R. Gomperts, R. E. Stratmann, O. Yazyev, A. J. Austin, R. Cammi, C. Pomelli, J. W. Ochterski, R. L. Martin, K. Morokuma, V. G. Zakrzewski, G. A. Voth, P. Salvador, J. J. Dannenberg, S. Dapprich, A. D. Daniels, O. Farkas, J. B. Foresman, J. V. Ortiz, J. Cioslowski, and D. J. Fox, Gaussian, Inc., Wallingford CT, 2009.

25. P. J. Stephens, F. J. Devlin, C. F. Chabalowski, and M. J. Frisch (1994). *J. Phys. Chem.* **98** (45), 11623–11627. https://doi.org/10.1021/j100096a001.
26. R. B. J. S. Krishnan, J. S. Binkley, R. Seeger, and J. A. Pople (1980). *J. Chem. Phys.* **72** (1), 650–654. https://doi.org/10.1063/1.438955.
27. A. Wang, Y. Wang, J. Jia, L. Feng, C. Zhang, and L. Liu (2013). *J. Phys. Chem. A.* **117**, 5061–5072. https://doi.org/10.1021/jp403145h.
28. S. F. Lo, S. Y. Wang, M. J. Tsai, and L. D. Lin (2020). *Chem. Eng. Res. Design* **90** (9), 1397–1406. https://doi.org/10.1016/j.cherd.2011.11.020.
29. L. Yang, D. R. Powell, and R. P. Houser (2007). *Dalton Trans.* **9**, 955–964. https://doi.org/10.1039/B617136B.
30. I. Chérif, M. F. Zid, M. El-Ghozzi, and D. Avignant (2012). *Acta Cryst*. https://doi.org/10.1107/S1600536812025020.
31. M. Chao, E. Schemp, and R. D. Rosenstein (1975). *Acta Cryst.* **B31** (12), 2924–2926. https://doi.org/10.1107/S0567740875009284.
32. S. Dgachi, M. M. Turnbull, F. Mezzadri, A. J. Norquist, A. Soran, J. Boonmak, G. Nemes, and H. Naïli (2021). *Inorganica Chim Acta*. https://doi.org/10.1016/j.ica.2020.119997.
33. S. Dgachi, F. Rahmouni, A. Soran, M. Saoudi, G. Nemes, and H. Naïli (2021). *J Mol Struct*. https://doi.org/10.1016/j.molstruc.2021.130996.
34. C. Orek, B. Gündüz, O. Kaygili, and N. Bulut (2017). *Chem. Phys. Lett.* **678**, 130–138. https://doi.org/10.1016/j.cplett.2017.04.050.
35. N. M. Juibari, A. Abbasi, M. Najafi, and S. Geranmayeh (2015). *C. R. Chimie* **18**, 662–667. https://doi.org/10.1016/j.crci.2014.11.006.
36. P. Raghunath, M. A. Reddy, C. Gouri, K. Bhanuprakash, and V. J. Rao (2006). *J. Phys. Chem. A.* **110**, 1152–1162. https://doi.org/10.1021/jp0555753.
37. A. M. B. Salah, R. P. Herrera, and H. Naïli (2018). *J. Mol. Struct.* **1165**, 356–362. https://doi.org/10.1016/j.molstruc.2018.04.002.
38. M. Rabiei, A. Palevicius, A. Monshi, S. Nasiri, A. Vilkauskas, and G. Janusas (2020). *Nanomaterials* **10** (9), 1627. https://doi.org/10.3390/nano10091627.
39. M. Bizi (2020). *Molecules* **25** (20), 4656. https://doi.org/10.3390/molecules25204656.
40. E. D. Revellame, D. L. Fortela, W. Sharp, R. Hernandez, and M. E. Zappi (2020). *Cleaner Eng Technol*. https://doi.org/10.1016/j.clet.2020.100032.
41. L. J. Martínez, A. Muñoz-Bonilla, E. Mazario, F. J. Recio, F. J. Palomares, and P. Herrasti (2015). *Int. J. Environ. Sci. Technol.* **12**, 4017–4024. https://doi.org/10.1007/s13762-015-0832-z.
42. V. K. Gupta, R. Chandra, I. Tyagi, and M. Verma (2016). *J. Colloid Interface Sci.* **478**, 54–62. https://doi.org/10.1016/j.jcis.2016.05.064.
43. S. K. Ashan, N. Ziaeifara, and M. Khosravi (2016). *Orient J Chem* **32** (1), 749–758. https://doi.org/10.13005/ojc/320184.